CRYSTAL GROWTH & DESIGN

pubs.acs.org/crystal

Communication

Highly Luminescent Metal–Organic Frameworks Based on Binary Chromophoric Ligands Derived from Tetraphenylethylene

Shanshan Mao, Yuhan Lin, Xingyu Li, and Hao Wang*

Cite This: https://doi.org/10.1021/acs.cgd.2c00441

Read Online

ACCESS | Metrics & More | Article Recommendations | Supporting Information

ABSTRACT: Two novel zinc-based metal–organic frameworks were constructed by employing tetraphenylethylene-derived tetracarboxylate/octacarboxylate ligands and a tetrapyridine linker, featuring a 3D porous framework. The two compounds display highly emissive green and blue-green luminescence, which may find uses in multichip LEDs.

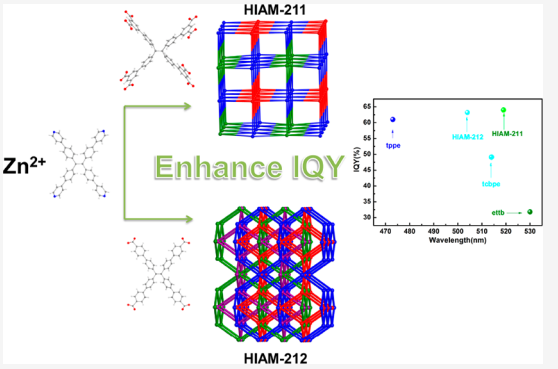

It is estimated that more than 50% of global electricity generation has been consumed by lighting and displays currently.[1,2] In this context, light-emitting materials with high efficiency have been brought into sharp focus on the scientific and commercial circles.[3] In consideration of their low power consumption, high efficiency, and long lifetime, light emitting diodes (LEDs) have been developed vigorously over the past decades.[4] One solution is that a near-ultraviolet LED chip (n-UV 380–420 nm) is coated with three phosphors that emit red, blue, and green, respectively, which supplies high-quality white light with excellent uniformity and high color rendering index (CRI).[5] Nevertheless, the existing commercial green phosphors suffer from weak chemical stability and harsh reaction conditions.[6] More importantly, the current phosphors largely rely on rare earth (RE) elements such as europium and cerium, leading to a surge in the price of RE metals over the past years.[7−9] Consequently, it is of great significance and urgency to develop RE-free green phosphors with high lighting efficiency.

The exceptional structural diversity as well as the theoretically countless combinations of the consisting metal ions and organic ligands make luminescent metal–organic frameworks (LMOFs) promising candidates for lighting or sensing related applications.[10,11] Concurrently, the selection of metal ions and organic ligands occupies an essential position in the construction of LMOFs.[12] The current RE-free LMOFs are generally constructed by means of combining organic chromophoric ligands with complementary metals that would not interfere with the emission properties of the ligands but act as nodes to connect and rigidify them in the extended structures.[13,14] Tetraphenylethylene (tpe) is known as a typical aggregation-induced emission (AIE) molecule, and its derivatives, especially the carboxylate form, tetrakis(4-carboxyphenyl)ethylene (H_4tcpe), have been extensively studied for the construction of LMOFs.[15,16] Metal ions with the d^{10} configuration (Zn^{2+}, Cd^{2+}, etc.) are commonly applied for building LMOFs, and Zn-MOFs are one of the most vital components.[17] In addition, LMOFs built on multiligand systems may have higher tunability with respect to their emission properties. For instance, employing a binary-ligand combination comprising an aromatic carboxylic and an N-donor linker can provide a flexible and diverse coordinate environment and display unique emitting behavior.[18,19]

We report here two novel LMOFs, [Zn_2(ettb)(tppe)] (HIAM-211) and [Zn(tcbpe)(tppe)] (HIAM-212) (ettb = 4′,4‴,4⁗,4⁗′-(1,1,2,2-ethenetetrayl)tetrakis(biphenyl-3,5-dicarboxylic acid), tcbpe = 1,1,2,2-tetrakis(4-(4-carboxyphenyl)phenyl)ethane, tppe = 1,1,2,2-tetrakis(4-pyridylphenyl)ethylene). The two new compounds HIAM-211 and HIAM-212 were synthesized by solvothermal reactions, and their structures have been characterized by single-crystal X-ray diffraction (SCXRD) analysis. Moreover, their optical properties were evaluated by photoluminescence (PL) and internal quantum yield (IQY).

Received: April 15, 2022
Revised: September 21, 2022

Yellow crystals of HIAM-211 were obtained from the reaction of H_8ettb, tppe, and $ZnCl_2$ in DMF at 100 °C for 24 h (see the Supporting Information for synthesis details). Single-crystal XRD demonstrated that it crystallizes in the tetragonal crystal system with the space group of *P*42/*nnm* (Table S1). The location of the solvent molecules is severely disordered and removed using the SQUEEZE routine of PLATON. Each of the two crystallographically independent Zn^{2+} centers is six-coordinated with four O atoms from two monodentate carboxylates and two bidentate carboxylates from four ettb ligands, and two N atoms from two separate tppe molecules, forming the binuclear secondary building unit (SBU) (Figure 1a, Figure S1). The bond lengths of Zn−O/N in the SBU are

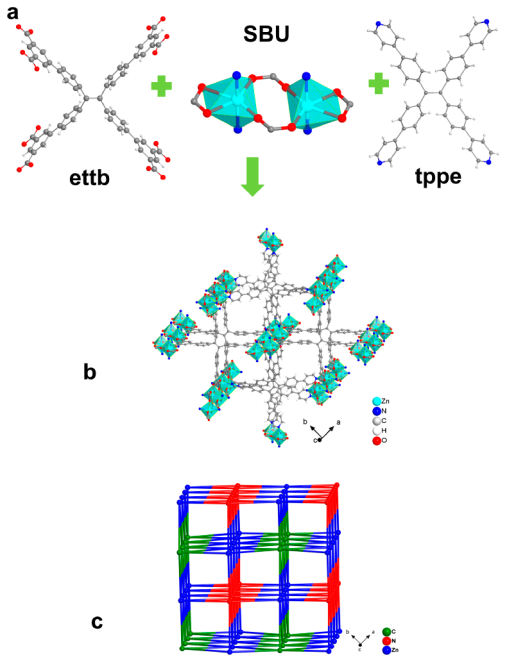

Figure 1. (a) Structure drawings for ettb and tppe ligands and secondary building unit of HIAM-211, (b) 3D structure of HIAM-211, and (c) the topological nets of HIAM-211.

in the range 1.984−2.345 Å, and the bond angles of O−Zn−O and O−Zn−N are approximately 89.03−155.47 and 85.78−94.98°, respectively (Tables S2 and S3). Bond valence sum analyses[20] and SHAPE software[21] are used to calculate the Zn(II) coordination polyhedron, giving a slightly distorted octahedral coordination configuration with deviation values of 4.520 (Tables S4 and S6). These SBUs are interconnected by ettb forming 2D layers on the ab plane, which are further pillared by tppe to construct the resultant 3D framework (Figure 1b). There are rectangular channels in the structure of HIAM-211 with a cross-section of approximately 9Å × 10Å. Further analysis reveals that it is a new topology with the Schläfli symbol of {4^18.6^10}2{4^20.6^8}{4^6}24,8,8-c (Figure 1c).

Crystals of HIAM-212 were obtained solvothermally from H_4tcbpe, tppe, and $ZnCl_2$ in DMF (150 °C for 48 h) with the addition of a small amount of HCl as a synthetic modulating agent. SCXRD revealed it crystallizes in the orthorhombic crystal system with space group *Ccce* (Table S1). Despite being composed of the same metal and similar ligands, the structure of HIAM-212 is totally different from that of HIAM-211. The Zn atom bonds to four oxygen atoms from two bidentate carboxylates from two different tcbpe linkers and two N atoms from two tppe ligands (Figure 2a, Figure S2). The four Zn−O

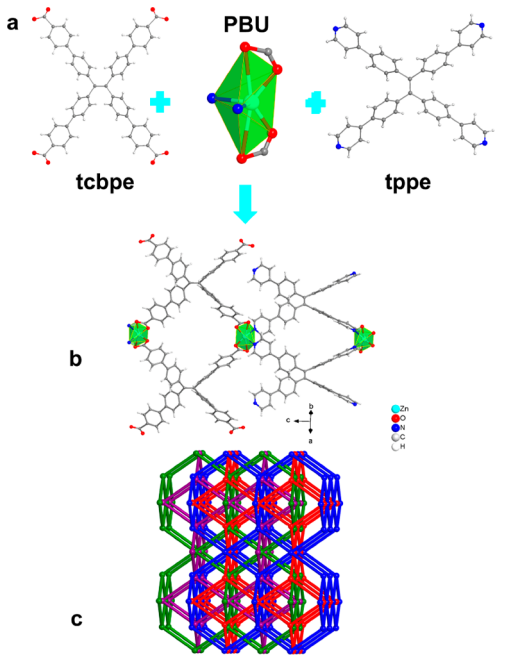

Figure 2. (a) Structure drawings for tppe and ettb ligands and primary building unit of HIAM-212, (b) structure of a single net of HIAM-212, and (c) 4-fold interpenetrated nets of HIAM-212.

bond lengths (1.979−2.246 Å) and two Zn−N distances (2.067 Å) are all within the reasonable range. The bond angles of O−Zn−O and O−Zn−N are approximately 94.2−121.1 and 110.7−120.3° (Tables S2 and S3). The results of bond valence theory indicate the Zn(II) is a distorted octahedral coordination corresponding to the calculation SHAPE software (Tables S5 and S7).[20,21] The framework is constructed from primary build units (PBUs) of $Zn(COO)_2N_2$. The PBUs are interconnected via tppe and tcbpe to form a 3D network, and four identical nets interlock with each other to form the resulting framework with 4-fold interpenetration (Figure 2b,c). A topology analysis reveals that the structure can be simplified as PTS topology denoted as 2-nodal (4, 4)-c net {4^2.8^4}.

The powder X-ray diffraction (PXRD) results show that the diffraction peaks of the two as-prepared zinc-based MOFs are consistent with the simulated patterns, confirming the phase purity of the samples (Figure 3). Thermogravimetric (TG) curves for both HIAM-211 and HIAM-212 display plateaus up to 350−400 °C following initial weight loss before 100 °C, indicating the structures are thermally robust (Figure S3). The porosity of the two compounds was characterized by N_2

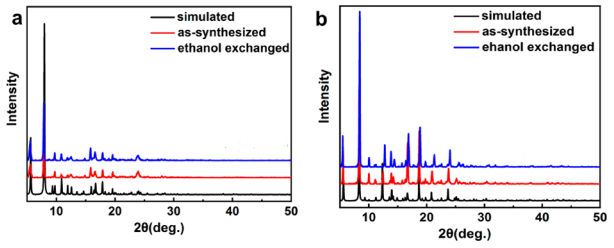

Figure 3. PXRD patterns of HIAM-211 (a) and HIAM-212 (b).

https://doi.org/10.1021/acs.cgd.2c00441
Cryst. Growth Des. XXXX, XXX, XXX−XXX

adsorption at 77 K. The saturated adsorption amounts for HIAM-211 and HIAM-212 are 326 and 249 cm^3/g, yielding BET surface areas of 1308 and 906 m^2/g, respectively (Figure S4).

Solid-state UV−vis absorption and photoluminescence spectra of ligands H_8ettb, H_4tcbpe, and tppe as well as the two MOFs were collected at room temperature. The UV−vis spectra illustrate that the absorption maxima of ettb, tppe, and tcbpe are at 389, 393, and 391 nm, respectively (Figure S5). The slight displacement of the HIAM-211and HIAM-212 is due to the $\pi-\pi^*$ transition.[17] As shown in Figure 4a−c,

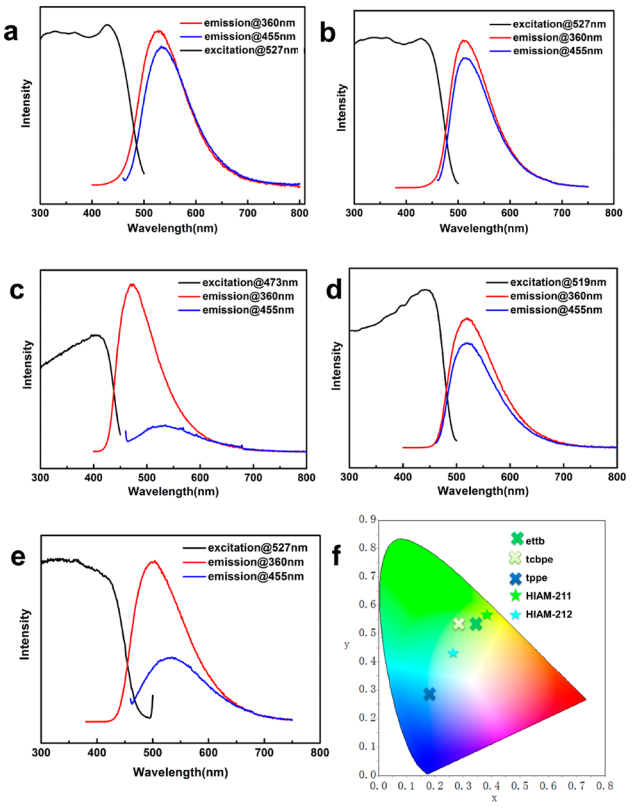

Figure 4. Optical properties of ettb, tcbpe, tppe, HIAM-211, and HIAM-212. Excitation and emission spectra of H8ettb (a), H4tcbpe (b), tppe (c), HIAM-211 (d), HIAM-212 (e), and CIE coordinates of ettb, tcbpe, tppe, HIAM-211, and HIAM-212 (f).

throughout a wide range of excitation energies, the emissions of H_8ettb, H_4tcbpe, and tppe fall right into the green/blue-green/blue region with peak wavelengths of 530, 514, and 417 nm, respectively. The excitation spectra of HIAM-211 and HIAM-212 are consistent with those of the organic linkers, and both compounds are UV- and blue-excitable. The two MOFs emit in the green and blue-green region. As shown in Figure 4d,e, the emission maxima are at 519 and 504 nm for HIAM-211 and HIAM-212, respectively, corresponding to blue-shifts of about 10 nm with regard to those of the chromophores (Table S8). That is possibly due to the disruption or reorganization of the delocalized conjugated system caused by the construction of the LMOF, which manifests the partial ligand-to-ligand charge transfer (LLCT).[19,22]

In addition, the optical emission is performed on as-made and outgassed HIAM-211 and HIAM-212 as well. It is worth noting that the emission peaks of outgassed HIAM-211′ and HIAM-212′ are red-shifted to 564 and 540 nm, respectively (Figure S6). The large red-shift of activated HIAM-211′ (34 nm) and HIAM-212′ (26 nm) in comparison with that of HIAM-211 and HIAM-212 could be put down to increased intermolecular electronic coupling without the interference of solvent guest molecules.[16]

The internal quantum yields (IQYs) measured under UV/blue (λ_{ex} = 365/450 nm) are 64% and 53.9% for HIAM-211 and 63.2% and 61.3% for HIAM-212, respectively. The quantum yields of HIAM-211′ and HIAM-212′ are 45% and 77%, respectively, under UV excitation (365 nm), indicating modulation of fluorescence by dual chromophores and stronger immobilization of H_4tcbpe (increase of quantum yield).[22] It can been seen from Tables S8 and S10 that these values are higher than those of the organic chromophores, some tcp-based MOFs and garnet material ($[Cd_2(tppe)\text{-}(2,6\text{-}ndc)2]\cdot 12DMF$ (47.2%), $[Cd(tcbpe)]\cdot(MeCN)$ (60.7%) and $Ca_{1.7}Y_{1.3}Zr_{1.7}Al_{3.3}O_{12}:0.03Ce^{3+}$ (53.4%) and $Ca_{1.99}LuZrScAl_2GeO_{12}:0.01Ce^{3+}$ (18.9%)). Moreover, in contrast with commercial green phosphor β-sialon:Eu^{2+} with a quantum efficiency of 52.2% when excited at 450 nm, HIAM-211, HIAM-212, and HIAM-212′ show higher efficiency as well.[23] The increase in quantum yields should be attributed to restriction of the rotation and torsion of the phenyl ring of the organic molecules in the extended structures.[16]

In order to study how temperature would influence the optical properties of HIAM-211 and HIAM-212, their photofluorescence at low and high temperature was evaluated. As shown in Figure S7, the emission intensity of HIAM-212 decreased slightly as the temperature increased in the range of 77−297 K, showing a low temperature dependence. This is mainly attributed to the fact that the increase of temperature can increase the chance of intermolecular collision, leading to an increase in non-radiative transitions and a decrease in fluorescence.[23,24] Additionally, no notable shift to its emission peak was observed as a function of temperature. In contrast, photoluminescence of HIAM-211 exhibited a high dependence on temperature. The fluorescence intensity increases with temperature, which may be related to the lesser effect of non-radioactive transitions.[25] The red-shifts of emission were observed as temperature increased, which could be attributed to the decrease in energy level difference and enhancement of intermolecular coupling when temperature increases, resulting in a corresponding increase in emission wavelength.[26] Thermal stability is one of the important properties to consider before recommending phosphors for potential applications.[27] It can be observed from Figure S8 that the fluorescence intensity of HIAM-211 gradually decreased after being heated in the range 298−373 K. On the other hand, the luminescence intensity shows a gradual decrease when the HIAM-212 is heated and the phosphor still maintains 47% of the emitting intensity at 100 °C compared with the initial intensity (25 °C). Combined with the performance of HIAM-212 at low temperature, this indicates that HIAM-212 has better thermal stability than HIAM-211. In addition, the fluorescence intensity of HIAM-211 and HIAM-212 hardly changed after 120 h of placement, suggesting that both compounds with long-term stability are candidates for excellent phosphors.

The fluorescence lifetimes of H_8ettb, H_4tcbpe, HIAM-211, and HIAM-212 are 3.89, 3.47, 3.87, and 2.54 ns, respectively (Figure S9, Tables S9 and S10), which is similar to previous findings of other tpe-based MOFs (e.g., $[Cd_2(tppe)\text{-}(2,6\text{-}ndc)2]\cdot 12DMF$, Table S10). Notably, the decreased fluorescence lifetime of HIAM-212 may relate to its increased

https://doi.org/10.1021/acs.cgd.2c00441
Cryst. Growth Des. XXXX, XXX, XXX−XXX

stiffness and energy emission. In this case, the rigidity of the tcbpe ligand prevents the twisting of the molecule in the excited state, which is the typical relaxation path for similar structures. The increased stiffness further limits the degree of relaxation after excitation, resulting in shorter lifetimes and higher energy emissions.

Commission International de l'Eclairage (CIE) coordinates of H_8ettb, H_4tcbpe, tppe, HIAM-211, and HIAM-212 are (0.331, 0.545), (0.293, 0.546), (0.189, 0.278), (0.262, 0.441), and (0.371, 0.559), respectively (Figure 4f). HIAM-211 is closer to commercial green phosphors (LuAG:Ce^{3+} (0.372, 0.566), while HIAM-212 located at the blue-green region is similar to $Ca_{1.7}Y_{1.3}Zr_{1.7}Al_{3.3}O_{12}$:0.03$Ce^{3+}$ (0.257, 0.464), suggesting that both compounds are potential green phosphor candidates to obtain high color rendering index and high-quality white light.

In conclusion, two new LMOFs, HIAM-211 and HIAM-212, have been constructed from different combinations of a tpe-based tetracarboxylate/octacarboxylate ligand and another tpe-based tetrapyridine linker. HIAM-212 exhibits a 4-fold interpenetrating 3D porous structure, while HIAM-211 features a 3D column-layer framework. Both materials are UV- and blue-excitable green or blue-green emitters with internal IQYs of 64% and 63.2% and great thermal stability under 365 nm excitation, making them promising as lighting phosphors for n-UV LEDs.

■ ASSOCIATED CONTENT

Supporting Information

The Supporting Information is available free of charge at https://pubs.acs.org/doi/10.1021/acs.cgd.2c00441.

Detailed synthesis and crystal data of MOFs; PXRD, TGA, and gas adsorption results of MOFs; fluorescence lifetimes; etc. (PDF)

Accession Codes

CCDC 2159610 and 2159613 contain the supplementary crystallographic data for this paper. These data can be obtained free of charge via www.ccdc.cam.ac.uk/data_request/cif, or by emailing data_request@ccdc.cam.ac.uk, or by contacting The Cambridge Crystallographic Data Centre, 12 Union Road, Cambridge CB2 1EZ, UK; fax: +44 1223 336033.

■ AUTHOR INFORMATION

Corresponding Author

Hao Wang − *Hoffmann Institute of Advanced Materials, Shenzhen Polytechnic, Shenzhen, Guangdong 518055, China*; orcid.org/0000-0001-7732-778X; Email: wanghao@szpt.edu.cn

Authors

Shanshan Mao − *Hoffmann Institute of Advanced Materials, Shenzhen Polytechnic, Shenzhen, Guangdong 518055, China*

Yuhan Lin − *Hoffmann Institute of Advanced Materials, Shenzhen Polytechnic, Shenzhen, Guangdong 518055, China*

Xingyu Li − *Hoffmann Institute of Advanced Materials, Shenzhen Polytechnic, Shenzhen, Guangdong 518055, China*

Complete contact information is available at: https://pubs.acs.org/10.1021/acs.cgd.2c00441

Author Contributions

H.W. conceived the idea. S.M., Y.L., and X.L. conducted the materials synthesis and characterizations. The manuscript was written from contributions from all authors. S.M. and Y.L. contributed equally to this work.

Notes

The authors declare no competing financial interest.

■ ACKNOWLEDGMENTS

We thank the National Natural Science Foundation of China (21901166), Natural Science Foundation of Guangdong Province (2019A1515010692), and Shenzhen Science and Technology Program (JCYJ20190809145615620, RCYX20200714114539243, KCXFZ20211020163818026).

■ REFERENCES

(1) Meng, Q.; Zhu, Q.; Li, X.; Sun, X.; Li, J. G. New $Mg^{(2+)}$/$Ge^{(4+)}$-Stabilized $Gd_3Mg_xGe_xAl_{5-2x}O_{12}$:Ce Garnet Phosphor with Orange-Yellow Emission for Warm-White LEDs (x = 2.0−2.5). *Inorg. Chem.* **2021**, *60*, 9773−9784.

(2) Hakeem, D. A.; Pi, J. W.; Kim, S. W.; Park, K. New $Y_2LuCaAl_2SiO_{12}$:Ln (Ln = Ce^{3+}, Eu^{3+}, and Tb^{3+}) phosphors for white LED applications. *Inorg. Chem. Front.* **2018**, *5*, 1336−1345.

(3) Sun, L.; Devakumar, B.; Liang, J.; Wang, S.; Sun, Q.; Huang, X. Highly efficient Ce^{3+} → Tb^{3+} energy transfer induced bright narrowband green emissions from garnet-type $Ca_2YZr_2(AlO_4)_3$:Ce^{3+},Tb^{3+} phosphors for white LEDs with high color rendering index. *J. Mater. Chem. C* **2019**, *7*, 10471−10480.

(4) Shao, B.; Huo, J.; You, H. Prevailing Strategies to tune emission color of lanthanide-activated phosphors for WLED applications. *Adv. Opt. Mater.* **2019**, 1900319.

(5) Zhong, J.; Zhuang, W.; Xing, X.; Liu, R.; Li, Y.; Zheng, Y.; Hu, Y.; Xu, H. Synthesis, structure and luminescence properties of new blue-green-emitting garnet-type $Ca_3Zr_2SiGa_2O_{12}$:Ce^{3+} phosphor for near-UV pumped white-LEDs. *RSC Adv.* **2016**, *6*, 2155−2161.

(6) Cao, L.; Li, W.; Devakumar, B.; Ma, N.; Huang, X.; Lee, A. F. Full-Spectrum white light-emitting diodes enabled by an efficient broadband green-emitting $CaY_2ZrScAl_3O_{12}$:$Ce^{(3+)}$ Garnet Phosphor. *ACS Appl. Mater. Inter* **2022**, *14*, 5643−5652.

(7) Wang, Y.; Ding, J.; Wang, Y. $Ca_{2-x}Y_{1+x}Zr_{2-x}Al^{3+x}O_{12}$:$Ce^{3+}$: solid solution design toward the green emission garnet structure phosphor for near-UV LEDs and their luminescence properties. *J. Phys. Chem. C* **2017**, *121*, 27018−27028.

(8) Zhang, Y.; Li, X.; Li, K.; Lian, H.; Shang, M.; Lin, J. Interplay between local environments and photoluminescence of Eu^{2+}in $Ba_2Zr_2Si_3O_{12}$: blue shift emission, optimal bond valence and luminescence mechanisms. *J. Mater. Chem. C* **2015**, *3*, 3294−3303.

(9) Li, W.; Xie, R. J.; Zhou, T.; Liu, L.; Zhu, Y. Synthesis of the phase pure $Ba_3Si_6O_{12}N_2$:Eu^{2+} green phosphor and its application in high color rendition white LEDs. *Dalton Trans.* **2014**, *43*, 6132−6138.

(10) Diamantis, S. A.; Margariti, A.; Pournara, A. D.; Papaefstathiou, G. S.; Manos, M. J.; Lazarides, T. Luminescent metal-organic frameworks as chemical sensors: common pitfalls and proposed best practices. *Inorg. chem. front.* **2018**, *5*, 1493−1511.

(11) Hu, Z.; Deibert, B. J.; Li, J. Luminescent metal-organic frameworks for chemical sensing and explosive detection. *Chem. Soc. Rev.* **2014**, *43*, 5815−5840.

(12) Ma, L.; Feng, X.; Wang, S.; Wang, B. Recent advances in AIEgen-based luminescent metal-organic frameworks and covalent organic frameworks. *Mater. Chem. Front.* **2017**, *1*, 2474−2486.

(13) Huangfu, M.; Wang, M.; Lin, C.; Wang, J.; Wu, P. Luminescent metal-organic frameworks as chemical sensors based on "mechanism-response": a review. *Dalton Trans.* **2021**, *50*, 3429−3449.

(14) Xu, Y.; Tao, C. L.; Yu, M.; Xiong, Y.; Ouyang, Y. N.; Liu, X. G.; Zhao, Z. Tetraphenylethene-Based Luminescent Metal-Organic Framework for Effective Differentiation of cis/trans Isomers. *ACS Appl. Mater. Interfaces* **2020**, *12*, 35266−35272.

(15) Medishetty, R.; Nalla, V.; Nemec, L.; Henke, S.; Mayer, D.; Sun, H.; Reuter, K.; Fischer, R. A. A New Class of Lasing Materials:

Intrinsic Stimulated Emission from Nonlinear Optically Active Metal-Organic Frameworks. *Adv. Mater.* **2017**, *29*, 1605637.
(16) Hu, Z.; Huang, G.; Lustig, W. P.; Wang, F.; Wang, H.; Teat, S. J.; Banerjee, D.; Zhang, D.; Li, J. Achieving exceptionally high luminescence quantum efficiency by immobilizing an AIE molecular chromophore into a metal-organic framework. *Chem. Commun.* **2015**, *51*, 3045−3048.
(17) Guo, X. Y.; Dong, Z. P.; Zhao, F.; Liu, Z. L.; Wang, Y.-Q. Zinc(II)−organic framework as a multi-responsive photoluminescence sensor for efficient and recyclable detection of pesticide 2,6-dichloro-4-nitroaniline, Fe(III) and Cr(VI). *New J. Chem.* **2019**, *43*, 2353−2361.
(18) Lustig, W. P.; Wang, F.; Teat, S. J.; Hu, Z.; Gong, Q.; Li, J. Chromophore-Based Luminescent Metal-Organic Frameworks as Lighting Phosphors. *Inorg. Chem.* **2016**, *55*, 7250−7256.
(19) Wang, F.; Liu, W.; Teat, S. J.; Xu, F.; Wang, H.; Wang, X.; An, L.; Li, J. Chromophore-immobilized luminescent metal-organic frameworks as potential lighting phosphors and chemical sensors. *Chem. Commun.* **2016**, *52*, 10249−10252.
(20) Brese, N. E.; O'Keeffe, M. Bond-Valence Parameters for Solids. *Acta Crystallogr.* **1991**, *47*, 192−197.
(21) Liu, M. J.; Yuan, J.; Zhang, Y. Q.; Sun, H. L.; Liu, C. M.; Kou, H. Z. Chiral six-coordinate Dy(III) and Tb(III) complexes of an achiral ligand: structure, fluorescence, and magnetism. *Dalton Trans* **2017**, *46*, 13035−13042.
(22) Wang, F.; Zhou, Z.; Liu, W.; Zhou, L.; Chen, L.; Li, J. Two blue-light excitable yellow-emitting LMOF phosphors constructed by triangular tri(4-pyridylphenyl)amine. *Dalton Trans.* **2017**, *46*, 956−961.
(23) Li, S.; Wang, L.; Tang, D.; Cho, Y.; Liu, X.; Zhou, X.; Lu, L.; Zhang, L.; Takeda, T.; Hirosaki, N.; Xie, R. J. Achieving high quantum efficiency narrow-band β-Sialon:Eu^{2+} phosphors for high-brightness LCD backlights by reducing the Eu^{3+} Luminescence Killer. *Chem. Mater.* **2018**, *30*, 494−505.
(24) Ren, K.; Xu, X.; Yao, Z.; Chen, X.; Hu, T.; Li, P.; Fan, X.; Du, J.; Qiao, X.; Qian, G. Temperature dependent molecular fluorescence of $[Agm]^{(n+)}$ quantum clusters stabilized by phosphate glass networks. *Phys. Chem. Chem. Phys.* **2020**, *22*, 21307−21316.
(25) Shustova, N. B.; Cozzolino, A. F.; Reineke, S.; Baldo, M.; Dinca, M. Selective turn-on ammonia sensing enabled by high-temperature fluorescence in metal-organic frameworks with open metal sites. *J. Am. Chem. Soc.* **2013**, *135*, 13326−13329.
(26) Wei, Z.; Gu, Z. Y.; Arvapally, R. K.; Chen, Y. P.; McDougald, R. N., Jr.; Ivy, J. F.; Yakovenko, A. A.; Feng, D.; Omary, M. A.; Zhou, H. C. Rigidifying fluorescent linkers by metal-organic framework formation for fluorescence blue shift and quantum yield enhancement. *J. Am. Chem. Soc.* **2014**, *136*, 8269−8276.
(27) Wang, H.; Zhu, Z.; Ma, B.; Wei, L.; Li, L. Improved thermal stability and luminescence properties of $SrSi_2O_2N_2$:Eu^{2+} green phosphor by a heterogeneous precipitation protocol for solid-state lighting applications. *Ceram. Int.* **2021**, *47*, 24163−24169.

https://doi.org/10.1021/acs.cgd.2c00441
Cryst. Growth Des. XXXX, XXX, XXX−XXX